Observational Study

Medicine®

OPEN

Quantitative analysis of anatomical relationship between cavernous segment internal carotid artery and pituitary macroadenoma

Bon-Jour Lin, MD[a,*], Tzu-Tsao Chung, MD[a], Meng-Chi Lin, MD[a], Chin Lin, Dr, Ph[c], Dueng-Yuan Hueng, MD, PhD[a], Yuan-Hao Chen, MD, PhD[a], Chung-Ching Hsia, MD[b], Da-Tong Ju, MD[a], Hsin-I Ma, MD, PhD[a], Ming-Ying Liu, MD[a], Chi-Tun Tang, MD[a]

Abstract

Cavernous segment internal carotid artery (CSICA) injury during endoscopic transsphenoidal surgery for pituitary tumor is rare but fatal. The aim of this study is to investigate anatomical relationship between pituitary macroadenoma and corresponding CSICA using quantitative means with a sense to improve safety of surgery.

In this retrospective study, a total of 98 patients with nonfunctioning pituitary macroadenomas undergoing endoscopic transsphenoidal surgeries were enrolled from 2005 to 2014. Intercarotid distances between bilateral CSICAs were measured in the 4 coronal levels, namely optic strut, convexity of carotid prominence, median sella turcica, and dorsum sellae. Parasellar extension was graded and recorded by Knosp–Steiner classification.

Our findings indicated a linear relationship between size of pituitary macroadenoma and intercarotid distance over CSICA. The correlation was absent in pituitary macroadenoma with Knosp–Steiner grade 4 parasellar extension.

Bigger pituitary macroadenoma makes more lateral deviation of CSICA. While facing larger tumor, sufficient bony graft is indicated for increasing surgical field, working area and operative safety.

Abbreviations: CSICA = cavernous segment internal carotid artery, Gd = gadolinium, ICA = internal carotid artery, MRI = magnetic resonance imaging.

Keywords: endoscopic transsphenoidal, internal carotid artery, pituitary macroadenoma

1. Introduction

Endoscopic transsphenoidal surgery is one of standard techniques for pituitary adenoma. Among reported complications of endoscopy procedure, injury to the internal carotid artery (ICA) is a fatal complication with an incidence of 0.25% to 3.8%.[1–3] Parasellar ICA and sella turcica occupy the central portion of surgical field, and being familiar with surrounding structures is absolutely necessary. Several cadaveric and imaging studies have reported the feasibility of identified bony landmarks and normal ICA course during endoscopic transsphenoidal surgery.[4–10] Nevertheless, studies discussing the anatomical relationship between pituitary adenoma and parasellar ICA are limited.

Preoperative assessment of association between pituitary adenoma and actual ICA course is important to minimize risk of ICA injury. Due to flattened view of 2-dimensional endoscopic surgery, modification of ICA nomenclature has been adopted for endoscopic surgery.[8,11–14] DePowell et al[13] proposed a modified ICA nomenclature suitable for both transcranial and endoscopic approaches and separated the cavernous segment ICA (CSICA) into 3 portions—C3-C4 bend, C4 segment, and C4-C5 bend.

Knowing anatomy of 3 portions of CSICA and their relationship with pituitary adenoma is suggested to assist surgeons in avoiding intraoperative ICA damage. Nevertheless, studies that examine the correlation of anatomic characteristics with CSICA in endoscopic perspective are limited. The aim of this study is to quantitatively analyze and examine the anatomical relationship between pituitary adenoma and corresponding parasellar ICA, named by DePowell's modified endoscopic classification.

2. Methods

2.1. Patient demographics

From January 2005 to December 2014, 129 endoscopic transsphenoidal operations for pituitary adenomas were performed in our institution (Tri-Service General Hospital, National Defense Medical Center). All procedures were approved by Taiwan neurosurgical society. For each tumor, functional status and permanent diagnosis were confirmed by hormone testing and histopathology respectively. Patients with nonfunctioning pituitary macroadenomas were eligible. Those with hormonally active

Editor: Anser Azim.

The authors have no funding and conflicts of interest to disclose.

[a] Department of Neurological Surgery, Tri-Service General Hospital, [b] Department of Surgery, Tri-Service General Hospital Songshan Branch, [c] Graduate Institute of Life Sciences, National Defense Medical Center, Taipei, Taiwan, R.O.C.

[*] Correspondence: Bon-Jour Lin, Department of Neurologic Surgery, Tri-Service General Hospital, Neihu, Taipei, Taiwan, R.O.C.
(e-mail: coleman0719@gmail.com).

Medicine (2016) 95:41(e5027)

Received: 24 April 2016 / Received in final form: 31 August 2016 / Accepted: 1 September 2016

http://dx.doi.org/10.1097/MD.0000000000005027

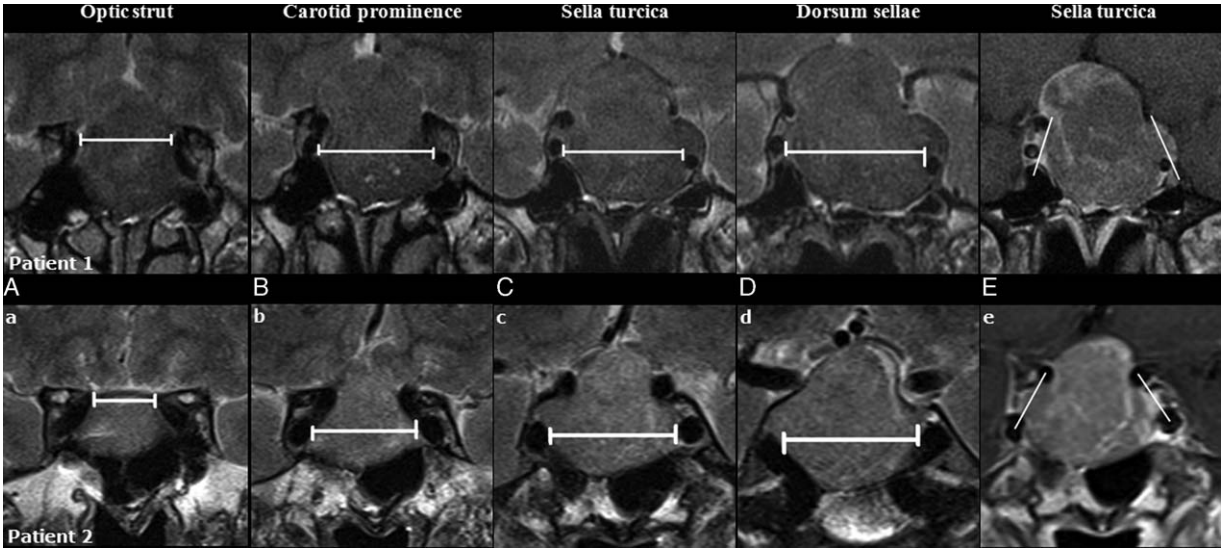

Figure 1. MRI of 2 patients with pituitary macroadenomas. For each patient, intercarotid distances (horizontal lines) were measured between medial walls of bilateral cavernous segment ICAs in 4 coronal levels: (A and a) at the optic strut; (B and b) at the convexity of carotid prominence; (C and c) at the median sella turcica; (D and d) at the dorsum sellae. Grading of parasellar extension was estimated by Knosp–Steiner classification on coronal contrast-enhanced images. (E) Patient 1, grade 3 on the left side and grade 0 on the right side. (e) Patient 2, grade 1 on the left side and grade 2 on the right side. ICA = internal carotid artery, MRI = magnetic resonance imaging.

tumors, previous pituitary surgery, previous pituitary radiosurgery, and incomplete MRI studies were excluded. A total of 98 patients were enrolled, including 65 males and 33 females with a mean age at the time of surgery of 51.18 years (range 13–87 years).

2.2. MRI acquisition

Preoperative MRI was performed on each patient using a 1.5-T MR unit (Vision Plus, Siemens). The MRI protocol was described as following: TR 2140 ms, TE 30 ms, TI 420 ms, matrix size 256×256, section thickness 2 mm, and intersection gap 0.21 mm. Routine images of the whole brain, including spin echo T1-weighted images, spin echo T2-weighted images, and fluid-attenuated inversion recovery (FLAIR) images were obtained. Spin echo contrast-enhanced T1-weighted images were obtained in the coronal, sagittal, and axial planes after intravenous gadolinium (Gd) administration (0.1 mmol/kg body weight).

2.3. Imaging measurement

1. Size of pituitary macroadenoma was assessed by 2 parameters on T1-weighted Gd-enhanced images: dimension of tumor in the coronal plane of median sella turcica; height of tumor in the midsagittal plane.
2. Distances between medial walls of bilateral cavernous segment internal carotid arteries (CSICAs) in 4 coronal planes from anterior to posterior: level 1, at the optic strut; level 2, at the convexity of carotid prominence; level 3, at the level of median sella turcica; level 4, at the dorsum sellae (Fig. 1).
   - For each patient, the coronal dimension of tumor in the coronal plane of median sella turcica and measured distances between medial walls of bilateral CSICAs in 4 coronal levels were divided into right and left components separately by extension of septum pellucidum. Definitions of distances measured in this study were shown in Table 1 and Fig. 2.

Table 1

Definitions of distances measured in this study.

Parameter*	Definition*
Point 1	Junction of cavernous segment ICA (CSICA) and clinoid segment ICA Correspond to DePowell's end of C4-C5 bend
Point 2	Junction of horizontal portion and anterior ascending portion of CSICA Correspond to DePowell's end of C4 segment and beginning of C4-C5 bend
Point 3	Median of horizontal portion of CSICA Correspond to DePowell's median of C4 segment
Point 4	Junction of posterior ascending portion and horizontal portion of CSICA Correspond to DePowell's end of C3-C4 bend and beginning of C4 segment
D1	Distance between bilateral point 1 (at the coronal level of optic strut)
D1-L (R)	Distance from left (right) point 1 to midline (at the coronal level of optic strut)
D1-dif.	Difference between D1-L and D1-R
D2	Distance between bilateral point 2 (at the coronal level of carotid prominence)
D2-L (R)	Distance from left (right) point 2 to midline (at the coronal level of carotid prominence)
D2-dif.	Difference between D2-L and D2-R
D3	Distance between bilateral point 3 (at the coronal level of median sella turcica)
D3-L (R)	Distance from left (right) point 3 to midline (at the coronal level of median sella turcica)
D3-dif.	Difference between D3-L and D3-R
D4	Distance between bilateral point 4 (at the coronal level of dorsum sellae)
D4-L (R)	Distance from left (right) point 4 to midline (at the coronal level of dorsum sellae)
D4-dif.	Difference between D4-L and D4-R

CSICA = cavernous segment internal carotid artery, ICA = internal carotid artery.
* See 3 orthogonal MRA images for pituitary macroadenoma (Fig. 1).

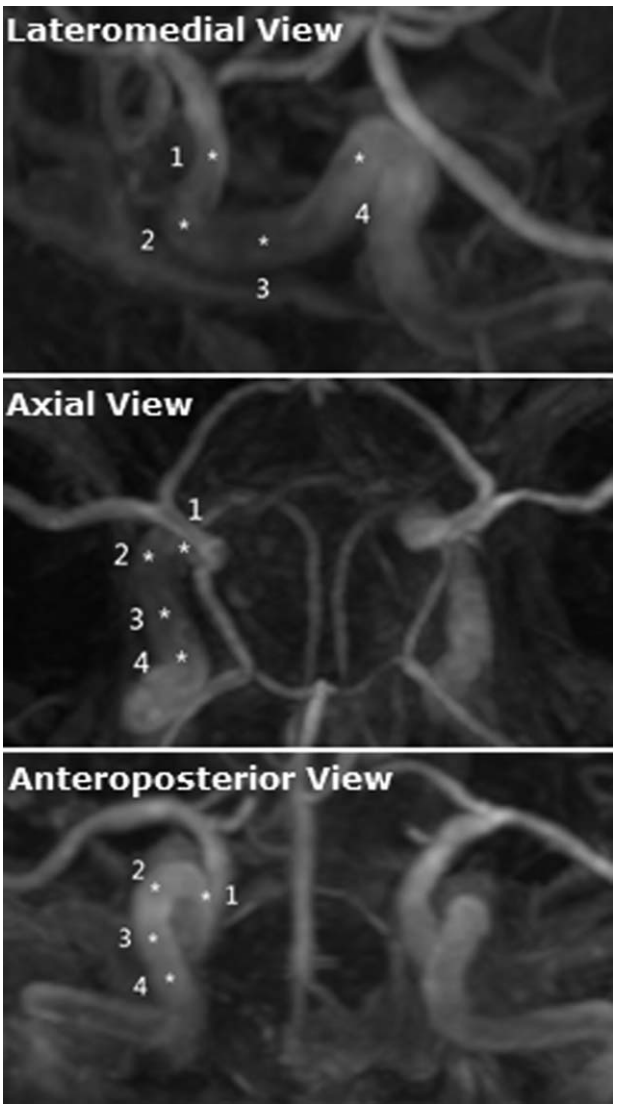

Figure 2. Three orthogonal MRA images for pituitary macroadenoma. MRA = magnectic resonance angiography.

3. Differences between left-sided and right-sided CSICA lateral deviation (distance measured from medial wall CSICA to midline) in 4 coronal levels.
4. Grading of parasellar extension of each tumor was evaluated by Knosp–Steiner classification on both sides in the coronal plane of median sella turcica.

2.4. Imaging analysis

The anatomical relationship between pituitary macroadenoma and CSICA was analyzed by following perspectives: (1) association between tumor size (including coronal dimension and sagittal height) and distances between bilateral CSICAs in 4 coronal levels; (2) association between tumor size and the difference between left-sided and right-sided CSICA lateral deviation in 4 coronal levels; (3) association between coronal dimension of tumor on one side and ipsilateral ICA lateral deviation in 4 coronal levels. The impact of different grading of parasellar extension was analyzed.

Table 2

Results of radiographic measurements in 98 pituitary macroadenomas.

Radiographics	Mean ± SD (mm)	Range (mm)
Tumor–sagittal height	26.00 ± 9.40	9.3–56.6
Tumor–coronal dimension	26.26 ± 6.68	15.5–48.5
Left-sided component	13.90 ± 4.39	6.0–27.9
Right-sided component	12.36 ± 4.43	4.2–23.8
D1*	16.36 ± 3.18	9.5–25.2
D1-L*	8.51 ± 2.11	4.1–13.5
D1-R*	7.93 ± 2.33	3.5–17.2
D1-dif.*	2.79 ± 1.67	0.3–7.6
D2*	24.22 ± 3.72	16.4–36.6
D2-L*	12.71 ± 2.44	7.5–18.9
D2-R*	11.46 ± 2.44	6.4–18.4
D2-dif.*	2.99 ± 2.34	0.1–10.5
D3*	23.69 ± 4.05	12.9–35.5
D3-L*	12.39 ± 2.72	5.3–18.8
D3-R*	11.31 ± 2.70	2.1–19.7
D3-dif.*	3.07 ± 2.59	0.1–12.2
D4*	23.00 ± 4.39	12.9–35
D4-L*	11.97 ± 2.72	4.9–18.8
D4-R*	11.05 ± 3.04	2.1–20.2
D4-dif.*	3.14 ± 2.68	0.1–12.2

SD = standard deviation.
* Definitions of measured distances are listed in Table 1.

2.5. Statistical analysis

All data were analyzed using the SPSS statistical program (version 20, IBM), and statistical significance was set at $P < 0.05$. The data of these measurements were presented as mean values ±SD of the mean. The difference in various parameters was analyzed with an independent samples t test and significant test. Pearson correlation coefficient was measured for the assessment of associations between continuous variables. While facing 2 predictive variables at the same time, standardized Regression Coefficients were used to assess the strength of the relationship.

3. Results

3.1. Size of pituitary macroadenomas

The height of macroadenoma in the midsagittal plane was 26 ± 9.4 mm (range 9.3–56.6 mm). The dimension of macroadenoma in the coronal level of median sella turcica was 26.26 ± 6.68 mm (range 15.5–48.5 mm). Each component was 13.9 ± 4.39 mm (range 6–27.9 mm) on the left side and 12.36 ± 4.43 mm (range 4.2–23.8 mm) on the right side. Results of radiographic measurements of 98 pituitary macroadenomas were shown in Table 2.

3.2. Measured distances over CSICAs

Distances between medial walls of bilateral CSICAs at the optic strut (D1), at the convexity of carotid prominence (D2), at the median sella turcica (D3) and at the dorsum sellae (D4) were 16.36 ± 3.18 mm (range 9.5–25.2 mm), 24.22 ± 3.72 (range 16.4–36.6 mm), 23.69 ± 4.05 mm (range 12.9–35.5 mm), and 23 ± 4.39 mm (range 12.9–35 mm) respectively.

Distances between medial wall of left CSICA and midline (left-sided CSICA lateral deviation) at the optic strut (D1-L), at the convex of carotid protuberance (D2-L), at the median sella turcica (D3-L) and at the dorsum sellae (D4-L) were 8.51 ± 2.11

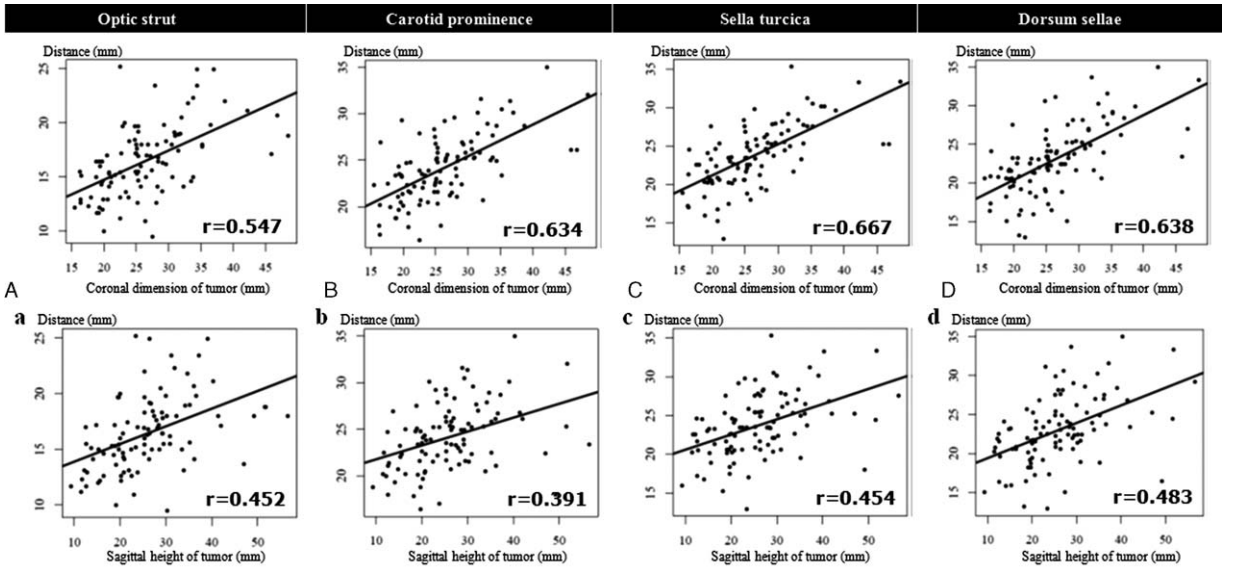

Figure 3. Regression analysis between size of pituitary macroadenoma (including coronal dimension and sagittal height) and intercarotid distances in 4 coronal levels. Relationship between coronal dimension of tumor and intercarotid distances at the optic strut (A, correlation coefficient (r) = 0.547); at the convexity of carotid prominence (B, r = 0.634); at the median sella turcica (C, r = 0.667); at the dorsum sellae (D, r = 0.638). Relationship between sagittal height of tumor and intercarotid distances at the optic strut (a, r = 0.452); at the convexity of carotid prominence (b, r = 0.391); at the median sella turcica (c, r = 0.454); at the dorsum sellae (d, r = 0.483).

mm (range 4.1–13.5 mm), 12.71 ± 2.44 mm (range 7.5–18.9 mm), 12.39 ± 2.72 mm (range 5.3–18.8 mm), and 11.97 ± 2.72 mm (range 4.9–18.8 mm). On the right side, the distances in 4 coronal planes were D1-R: 7.93 ± 2.33 mm (range 3.5–17.2 mm), D2-R: 11.46 ± 2.44 mm (range: 6.4–18.4 mm), D3-R: 11.31 ± 2.7 mm (range 2.1–19.7 mm), and D4-R: 11.05 ± 3.04 mm (range 2.1–20.2 mm).

Differences between left-sided and right-sided CSICA lateral deviation at the optic strut (D1-dif.), at the convex of carotid protuberance (D2-dif.), at the median sella turcica (D3-dif.), and at the dorsum sellae (D4-dif.) were 2.79 ± 1.67 mm (range 0.3–7.6 mm), 2.99 ± 2.34 (range 0.1–10.5 mm), 3.07 ± 2.59 mm (range 0.1–12.2 mm), and 3.14 ± 2.68 mm (range 0.1–12.2 mm), respectively.

3.3. Anatomical relationship between tumor and CSICA

The coronal dimension of pituitary macroadenoma was significantly associated with distances between medial walls of bilateral CSICAs in 4 coronal planes. The correlation coefficients were 0.547 at the level of optic strut; 0.634 at the level of convexity of carotid prominence; 0.667 at the level of median sella turcica and 0.638 at the level of dorsum sellae (Fig. 3, A–D). There was also a significant association between the height of pituitary macroadenoma and medial walls of bilateral CSICAs in 4 coronal planes (Fig. 3, A–D). The coronal dimension and height of pituitary macroadenoma were poorly correlated with difference between right-sided and left-sided CSICA lateral deviation in 4 coronal levels (Fig. 4).

For each side of macroadenoma, the strong association exists between dimension of tumor on 1 side and ipsilateral ICA lateral deviation in 4 coronal levels. The standardized regression coefficients were 0.502 at the level of optic strut; 0.615 at the level of convexity of carotid prominence; 0.691 at the median sella turcica and 0.666 at the level of dorsum sellae (Fig. 5).

3.4. Impact of grading of parasellar extension

Bilateral sides of parasellar extension were recorded for each patient. On the left side, amount of tumors with Knosp–Steiner grade 0, 1, 2, 3, 4 were 20, 40, 20, 11, and 7. On the right side, amount of tumors with grade 0, 1, 2, 3, 4 were 35, 31, 19, 5, and 8, respectively.

Coronal dimension of tumor and ICA lateral deviation in the 4 coronal levels with different grading of parasellar extension were shown in Table 3. Within each grading of parasellar extension, the relationship between coronal dimension of tumor and ICA lateral deviation in 4 coronal levels were expressed as Pearson correlation efficiencies (Table 4). Within grade 4 of parasellar extension, coronal dimension of tumor on one side is not correlated with ipsilateral ICA lateral deviation ($P > 0.05$).

4. Discussion

Being familiar with position of cavernous segment internal carotid artery (CSICA) within limited surgical field is important while performing endoscopic transsphenoidal approach. Intercarotid distances between patients with pituitary macroadenomas and healthy individuals were compared and significantly wider intercarotid distances were observed for those with pituitary macroadenomas.[15,16] Although quantitative analysis of distances between CSICAs while facing endoscopic transsphenoidal approaches were conducted, these studies failed to discuss the direct association between CSICA morphology and pituitary adenoma.[4,5,11,15–19] Measurements from cadaveric study and those from image study existed significant difference.[16]

Commonly accepted classification of ICA is based on direction of antegrade flow and surrounding anatomy through dorsolateral transcranial approach, and the most used form, proposed by Bouthillier et al,[20–22] separates the ICA into 7 segments. The cavernous segment ICA is further divided into 5 portions,

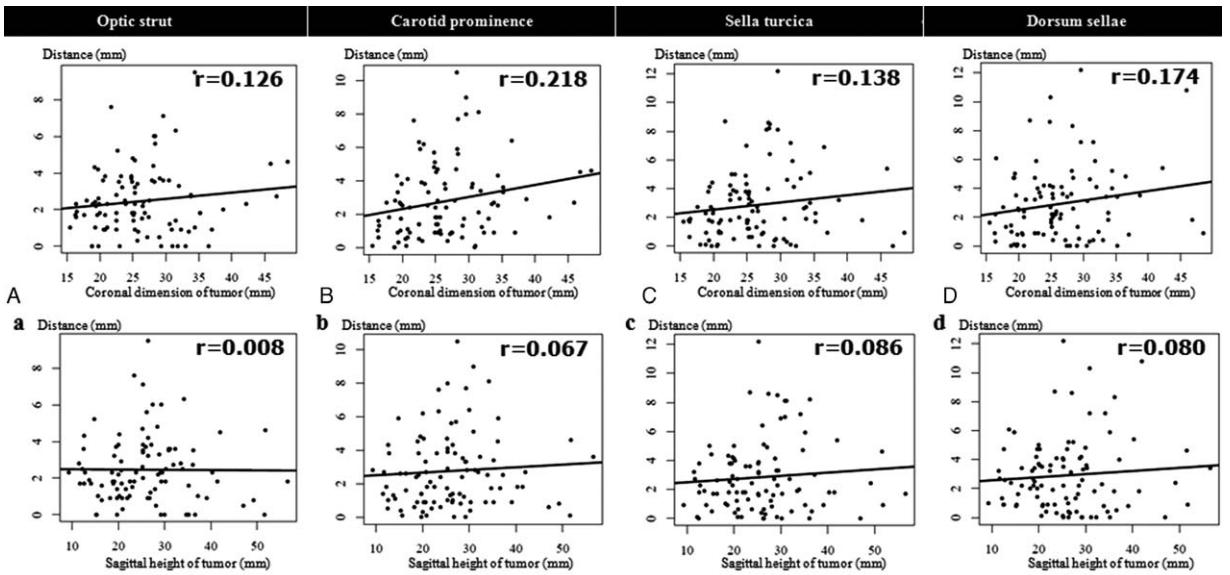

Figure 4. Regression analysis between size of pituitary macroadenoma (including coronal dimension and sagittal height) and differences of left-sided and right-sided ICA lateral deviation in 4 coronal levels. Relationship between coronal dimension of tumor and differences of bilateral ICA lateral deviation at the optic strut (A, correlation coefficient (r) = 0.126); at the convexity of carotid prominence (B, r = 0.218); at the median sella turcica (C, r = 0.138); at the dorsum sellae (D, r = 0.174). Relationship between sagittal height of tumor and differences of bilateral ICA lateral deviation at the optic strut (a, r = 0.008); at the convexity of carotid prominence (b, r = 0.067); at the median sella turcica (c, r = 0.086); at the dorsum sellae (d, r = 0.080). ICA = internal carotid artery.

described by Debrun et al[23]: (1) anterior ascending portion; (2) junction of anterior ascending and horizontal portion; (3) horizontal portion; (4) junction of horizontal and posterior ascending portion; (5) posterior ascending portion.

Traditional ICA nomenclature is ineligible and inappropriate for endoscopic transsphenoidal approach because of flat nature of 2-dimensional endoscopic view. Several modified classifications are announced for better understanding of ICA course through 2-dimensional endoscopic view.[8,11–13]

DePowell et al[13] proposed 1 revised classification of ICA, suitable for both transcranial and endoscopic approaches, as universal language between clinicians. Its description of the CSICA, including C3–4 bend, C4 segment, and C4–5 bend, is used in our study to represent different portion of intracavernous ICA while performing the endoscopic transsphenoidal approach. Four coronal levels of ICA measurement represent different portion of CSICA, respectively. ICA in the coronal level of optic strut, corresponding to DePowell's end of C4-C5 bend, is the site of junction of CSICA and clinoid segment ICA. Level of carotid prominence, corresponding to DePowell's end of C4 segment and beginning of C4-C5 bend, points to the transition from horizontal portion to anterior ascending portion. Level of median sella turcica, corresponding to DePowell's median of C4 segment, represents the horizontal portion. Level of dorsum sellae, corresponding to DePowell's end of C3-C4 bend and beginning of C4 segment, approximates the transition from posterior ascending portion to the horizontal portion.

Increased intercarotid distances between CSICA in patients with pituitary adenomas were reported by previous studies.[16,19] The result of our study elaborate on intercarotid distances being linearly proportional to size of pituitary macroadenomas—larger tumor causing wider intercarotid distances in 4 coronal levels of measurement, whole sella turcica. It is postulated that progressive enlargement of pituitary adenoma causing expansion of sella

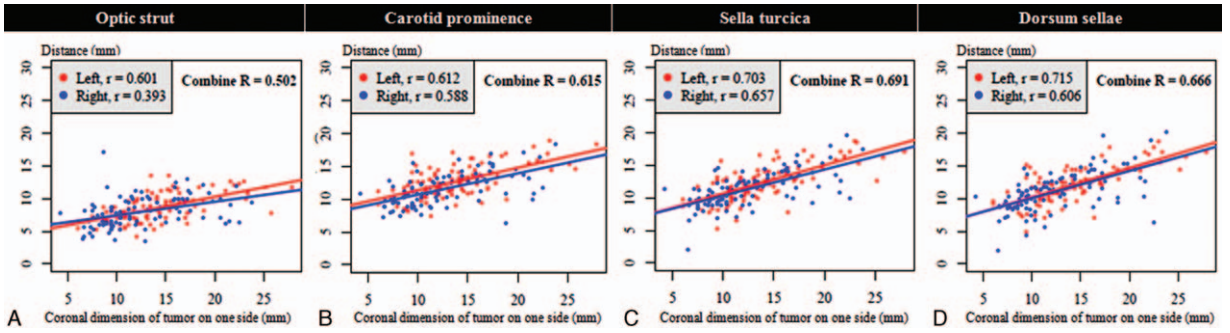

Figure 5. Regression analysis between coronal dimension of tumor on the one side and ipsilateral ICA lateral deviation in 4 coronal levels. Relationship between coronal dimension of tumor on the one side and ipsilateral ICA lateral deviation at the optic strut (A, standardized regression coefficient (R) = 0.502); at the convexity of carotid prominence (B, R = 0.615); at the median sella turcica (C, R = 0.691); at the dorsum sellae (D, R = 0.666). ICA = internal carotid artery.

Table 3

Radiographic measurements for pituitary macroadenomas with different grades of parasellar extension.

Radiographics	Knosp–Steiner Classification					$P^{\S}$
	Grade 0	Grade 1	Grade 2	Grade 3	Grade 4	
Left-sided tumor†	10.42 ± 2.76	12.21 ± 1.99	14.68 ± 2.96	19.75 ± 3.05	22.10 ± 4.41	<0.001
D1-L*	8.22 ± 2.30	7.95 ± 1.72	8.36 ± 2.29	10.45 ± 1.74	9.94 ± 1.88	0.002
D2-L*	12.84 ± 2.45	11.68 ± 1.73	13.01 ± 2.49	14.97 ± 2.54	13.80 ± 3.19	0.001
D3-L*	12.45 ± 2.40	11.60 ± 2.03	11.55 ± 2.90	15.36 ± 2.26	14.44 ± 3.55	<0.001
D4-L*	11.60 ± 2.15	11.20 ± 1.97	11.14 ± 2.76	15.14 ± 2.13	14.79 ± 3.90	<0.001
Right-sided tumor‡	9.13 ± 2.16	11.55 ± 2.93	14.46 ± 3.33	19.90 ± 2.19	19.89 ± 3.55	<0.001
D1-R*	7.55 ± 2.49	8.07 ± 2.17	8.36 ± 2.66	9.06 ± 2.09	7.38 ± 1.65	0.520
D2-R*	11.07 ± 1.97	11.08 ± 2.27	11.74 ± 2.89	14.60 ± 2.34	12.00 ± 2.97	0.030
D3-R*	10.70 ± 1.97	10.85 ± 2.31	11.89 ± 3.12	15.92 ± 3.55	11.43 ± 3.06	0.001
D4-R*	10.19 ± 2.08	10.96 ± 3.24	11.62 ± 3.08	14.70 ± 3.80	11.51 ± 4.08	0.026

Data of measurement is presented as mean value ± standard deviation of the mean, unit is millimeter.

* Definitions of measured distances are listed in Table 1.

† Left-sided component of tumor dimension at coronal level of median sella turcica.

‡ Right-sided component of tumor dimension at coronal level of median sella turcica.

§ Significance test for means between tumors with different grades of parasellar extension.

turcica and lateral deviation of cavernous sinus structure, including CSICA. Considering asymmetrical growth of pituitary macroadenoma may cause unpredicted CSICA lateral deviation, we divide the coronal dimension of tumor and measure intercarotid distances into right-sided and left-sided components. Existence of linear relationship between coronal dimension of tumor on one side and ipsilateral ICA lateral deviation in 4 coronal levels is also observed. Otherwise, differences between left-sided and right-sided CSICA lateral deviation in 4 coronal levels are not related to tumor size. By the above stated findings, we make 2 conclusions. The first, the amount of lateral deviation of CSICA over whole sella turcica is directly proportional to size of pituitary adenoma. The second, increased size of pituitary adenoma would not increase asymmetry of CSICA lateral deviation.

Cavernous sinus invasion by pituitary adenoma is considered as another issue with an incidence of 6% to 10%.[24,25] Preoperative investigation for cavernous sinus invasion by pituitary adenoma is important to reduce operative morbidity. Although intraoperative finding is the gold standard diagnosis for cavernous sinus invasion, multiple radiographic characteristics are suggested as predictors for cavernous sinus invasion preoperatively with different sensitivity and specificity.[26–29] Researches had highlighted that increased size of pituitary adenoma accompanied with higher risk of cavernous sinus invasion.[30,31] However, the impact of cavernous sinus invasion on CSICA morphology is still unknown. In this study, Knosp–Steiner classification is employed to categorize the grading of parasellar extension by pituitary macroadenoma. Grading of parasellar extension on both sides of pituitary adenomas in the coronal plane of median sella turcica is recorded and its association with tumor size and CSICA lateral deviation is analyzed.

By the result of the study, increased grading of parasellar extension of pituitary macroadenomas accompany with larger coronal dimensions and further CSICA lateral deviation. Pituitary adenoma with grade 4 parasellar extension does not get linear relationship between tumor size and ICA lateral deviation. Preoperatively getting information about size of pituitary adenoma, Knosp–Steiner grading of parasellar extension is important and helpful in predicting intraoperative CSICA morphology.

Table 4

Correlation coefficients between tumor size and lateral deviation of ICA for pituitary macroadenomas with different grades of parasellar extension.

	Knosp–Steiner classification										
	Grade 0		Grade 1		Grade 2		Grade 3		Grade 4		
	Pearson's $r^{\S}$	P value‖	Pearson's $r^{\S}$	P value‖	Pearson's $r^{\S}$	P value‖	Pearson's $r^{\S}$	P value§	Pearson's $r^{\S}$	P value‖	$P^{\P}$
D1-L*/tumor-L†	0.78	<0.001	0.54	<0.001	0.46	0.041	0.74	0.009	0.87	0.011	0.472
D2-L*/tumor-L†	0.81	<0.001	0.76	<0.001	0.91	<0.001	0.84	0.001	0.52	0.233	0.092
D3-L*/tumor-L†	0.42	0.062	0.75	<0.001	0.86	<0.001	0.84	0.001	0.55	0.197	0.070
D4-L*/tumor-L†	0.81	<0.001	0.37	0.018	0.61	0.005	0.68	0.022	0.44	0.323	0.109
D1-R*/tumor-R‡	0.38	0.024	0.55	0.001	0.81	<0.001	0.74	0.157	0.36	0.385	0.313
D2-R*/tumor-R‡	0.57	<0.001	0.82	<0.001	0.58	0.009	0.85	0.066	0.59	0.127	0.774
D3-R*/tumor-R‡	0.58	<0.001	0.75	<0.001	0.88	<0.001	0.98	0.003	0.73	0.039	0.023
D4-R*/tumor-R‡	0.56	<0.001	0.77	<0.001	0.76	<0.001	0.97	0.006	0.37	0.362	0.082

* Definitions of measured distances are listed in Table 1.

† Left-sided component of tumor dimension at coronal level of median sella turcica.

‡ Right-sided component of tumor dimension at coronal level of median sella turcica.

§ Correlation coefficient between tumor dimension and lateral deviation of ICA on the one side.

‖ Significance test for correlation coefficients between tumors with the same grade of parasellar extension.

¶ Significance test for correlation coefficients between tumors with different grades of parasellar extension.

Limitations of this study include small patient population, retrospective nature, and interobserver variability. In the future, larger patient number and prospective studies are needed to confirm the accuracy of this study.

5. Conclusion

Linear relationship exists between size of pituitary adenoma and intercarotid distance over CSICA—bigger tumor mass makes more lateral deviation of CSICA. While facing larger tumor, sufficient bony graft is indicated for increasing surgical field, working area, and operative safety. However, it is worth noting that this relationship does not exist in tumors with Knosp–Steiner grade 4 parasellar extension.

References

[1] Ciric I, Ragin A, Baumgartner C, et al. Complications of transsphenoidal surgery: results of a national survey, review of the literature, and personal experience. Neurosurgery 1997;40:225–36.

[2] Dusick JR, Esposito F, Malkasian D, et al. Avoidance of carotid artery injuries in transsphenoidal surgery with the Doppler probe and micro-hook blades. Neurosurgery 2007;60:322–8.

[3] Gardner PA, Tormenti MJ, Pant H, et al. Carotid artery injury during endoscopic endonasal skull base surgery: incidence and outcomes. Neurosurgery 2013;73: ons261-269.

[4] Cheng Y, Zhang H, Su L, et al. Anatomical study of cavernous segment of the internal carotid artery and its relationship to the structures in sella region. J Craniofac Surg 2013;24:622–5.

[5] Feng Y, Zhao JW, Liu M, et al. Internal carotid artery in the operative plane of endoscopic endonasal transsphenoidal surgery. J Craniofac Surg 2012;23:909–12.

[6] Kassam AB, Gardner PA, Snyderman CH, et al. Expanded endonasal approach, a fully endoscopic transnasal approach for the resection of midline suprasellar craniopharyngiomas: a new classification based on the infundibulum. J Neurosurg 2008;108:715–28.

[7] Labib MA, Prevedello DM, Fernandez-Miranda JC, et al. The medial opticocarotid recess: an anatomic study of an endoscopic "key landmark" for the ventral cranial base. Neurosurgery 2013;72: 66–76.

[8] Labib MA, Prevedello DM, Carrau R, et al. A road map to the internal carotid artery in expanded endoscopic endonasal approaches to the ventral cranial base. Neurosurgery 2014;10:448–71.

[9] Peris-Celda M, Kucukyuruk B, Monroy-Sosa A, et al. The recesses of the sellar wall of the sphenoid sinus and their intracranial relationships. Neurosurgery 2013;73: ons117-131.

[10] Zhang SJr, Tian Y, Wu D, et al. Measurement of safety range in primary nasal transsphenoidal approach for pituitary surgery. J Craniofac Surg 2013;24:617–8.

[11] Alfieri A, Jho HD. Endoscopic endonasal cavernous sinus surgery: an anatomic study. Neurosurgery 2001;48:827–36.

[12] Cebula H, Kurbanov A, Zimmer LA, et al. Endoscopic, endonasal variability in the anatomy of the internal carotid artery. World Neurosurg 2014;82:e759–64.

[13] DePowell JJ, Froelich SC, Zimmer LA, et al. Segments of the internal carotid artery during endoscopic transnasal and open cranial approaches: can a uniform nomenclature apply to both? World Neurosurg 2014;82:S66–71.

[14] Herzallah IR, Casiano RR. Endoscopic endonasal study of the internal carotid artery course and variations. Am J Rhinol 2007;21:262–70.

[15] Scotti G, Yu CY, Dillon WP, et al. MR maging of cavernous sinus involvement by pituitary adenomas. AJR Am J Roentgenol 1988;151: 799–806.

[16] Yilmazlar S, Kocaeli H, Eyigor O, et al. Clinical importance of the basal cavernous sinuses and cavernous carotid arteries relative to the pituitary gland and macroadenomas: quantitative analysis of the complete anatomy. Surg Neurol 2008;70:165–74.

[17] Inoue T, Rhoton ALJr, Theele D, et al. Surgical approaches to the cavernous sinus: a microsurgical study. Neurosurgery 1990;26:903–32.

[18] Kayalioglu G, Govsa F, Erturk M, et al. The cavernous sinus: topographic morphometry of its contents. Surg Radiol Anat 1999;21:255–60.

[19] Sasagawa Y, Tachibana O, Doai M, et al. Internal carotid arterial shift after transsphenoidal surgery in pituitary adenomas with cavernous sinus invasion. Pituitary 2013;16:465–70.

[20] Bouthillier A, van Loveren HR, Keller JT. Segments of the internal carotid artery: a new classification. Neurosurgery 1996;38:425–32.

[21] Rhoton ALJr. The supratentorial arteries. Neurosurgery 2002;51: S53–120.

[22] Ziyal IM, Ozgen T, Sekhar LN, et al. Proposed classification of segments of the internal carotid artery: anatomical study with angiographical interpretation. Neurol Med Chir (Tokyo) 2005;45:184–90.

[23] Debrun G, Lacour P, Vinuela F, et al. Treatment of 54 traumatic carotid-cavernous fistulas. J Neurosurg 1981;55:678–92.

[24] Ahmadi J, North CM, Segall HD, et al. Cavernous sinus invasion by pituitary adenomas. Am J Roentgenol 1986;146:257–62.

[25] Fahlbusch R, Buchfelde M. Transsphenoidal surgery of parasellar pituitary adenomas. Acta Neurochir (Wien) 1988;92:93–9.

[26] Sol YL, Lee SK, Choi HS, et al. Evaluation of MRI criteria for cavernous sinus invasion in pituitary macroadenoma. J Neuroimaging 2014;24:498–503.

[27] Vieira JOJr, Cukiert A, Liberman B. Magnetic resonance imaging of cavernous sinus invasion by pituitary adenoma diagnostic criteria and surgical findings. Arq Neuropsiquiatr 2004;62:437–43.

[28] Vieira JOJr, Cukiert A, Liberman B. Evaluation of magnetic resonance imaging criteria for cavernous sinus invasion in patients with pituitary adenomas: logistic regression analysis and correlation with surgical findings. Surg Neurol 2006;65:130–5.

[29] Yoneoka Y, Watanabe N, Matsuzawa H, et al. Preoperative depiction of cavernous sinus invasion by pituitary macroadenoma using three-dimensional anisotropy contrast periodically rotated overlapping parallel lines with enhanced reconstruction imaging on a 3-tesla system. J Neurosurg 2008;108:37–41.

[30] Knosp E, Steiner E, Kitz K, et al. Pituitary adenomas with invasion of the cavernous sinus space: a magnetic resonance imaging classification compared with surgical findings. Neurosurgery 1993;33:610–7.

[31] Selman WR, Laws ERJr, Scheithauer BW, et al. The occurrence of dural invasion in pituitary adenomas. J Neurosurg 1986;64:402–7.